nanomaterials

MDPI

# Supplementary Materials

# Rationally Designed CdS-Based Ternary Heterojunctions: A Case of 1T-$MoS_2$ in CdS/$TiO_2$ Photocatalyst

**Wenqian Chen [1,3,*,†], Shaomei Zhang [1,2,†], Ganyu Wang [1,2], Gang Huang [4], Zhichong Yu [1,2], Yirui Li [1,2] and Liang Tang [1,2,*]**

[1] Key Laboratory of Organic Compound Pollution Control Engineering, Ministry of Education, Shanghai 200444, China
[2] School of Environmental and Chemical Engineering, Shanghai University, Shanghai 200444, China; shaomeizhang@shu.edu.cn (S.Z.); wgy@shu.edu.cn (G.W.); zhichongyu@shu.edu.cn (Z.Y.); yiruili@shu.edu.cn (Y.L.)
[3] Shanghai Institute of Applied Radiation, Shanghai University, 20 Chengzhong Road, Shanghai 201800, China
[4] Physical Science and Engineering Division King Abdullah University of Science and Technology (KAUST), Thuwal 23955-6900, Saudi Arabia; gang.huang@kaust.edu.sa
* Correspondence: wenqianchen@shu.edu.cn (W.C.); tang1liang@shu.edu.cn (L.T.)
† Equal contribution.

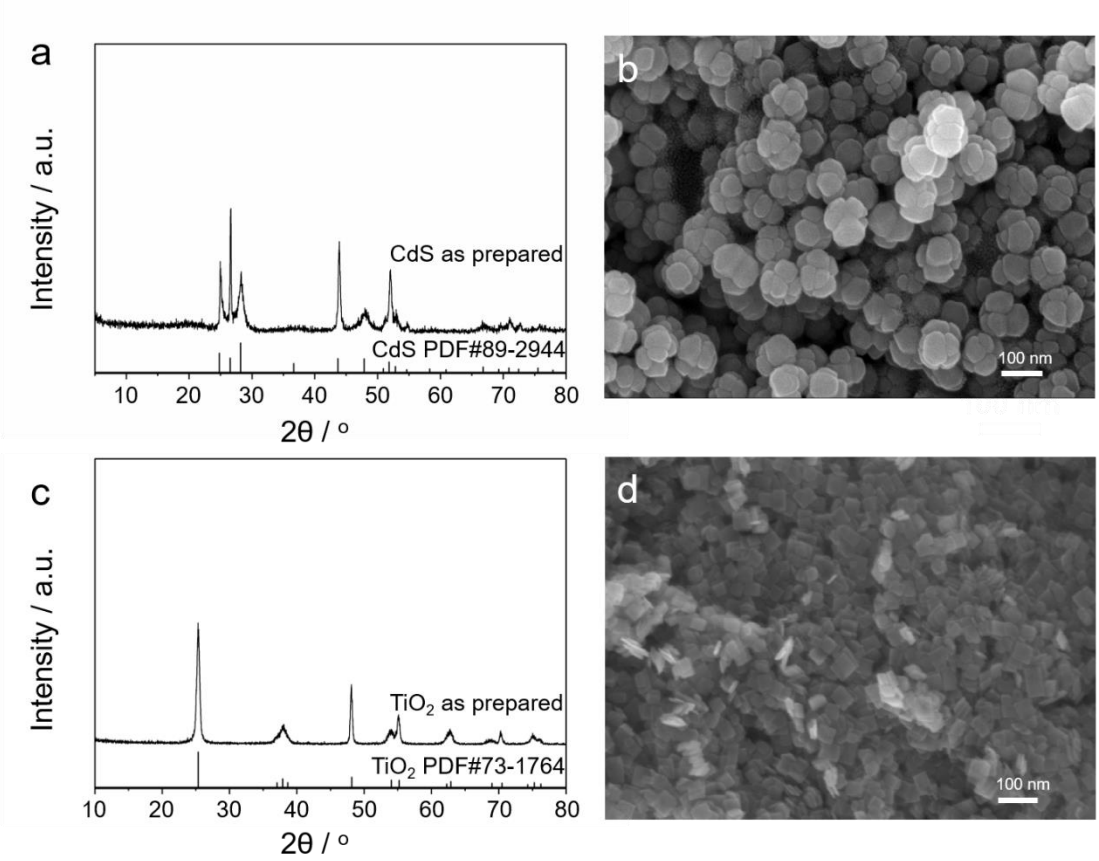


**Figure S1.** (**a**) XRD pattern and (**b**) SEM image of the pure CdS nanoparticles, (**c**) XRD pattern and (**d**) SEM image of the $TiO_2$ nanosheets.

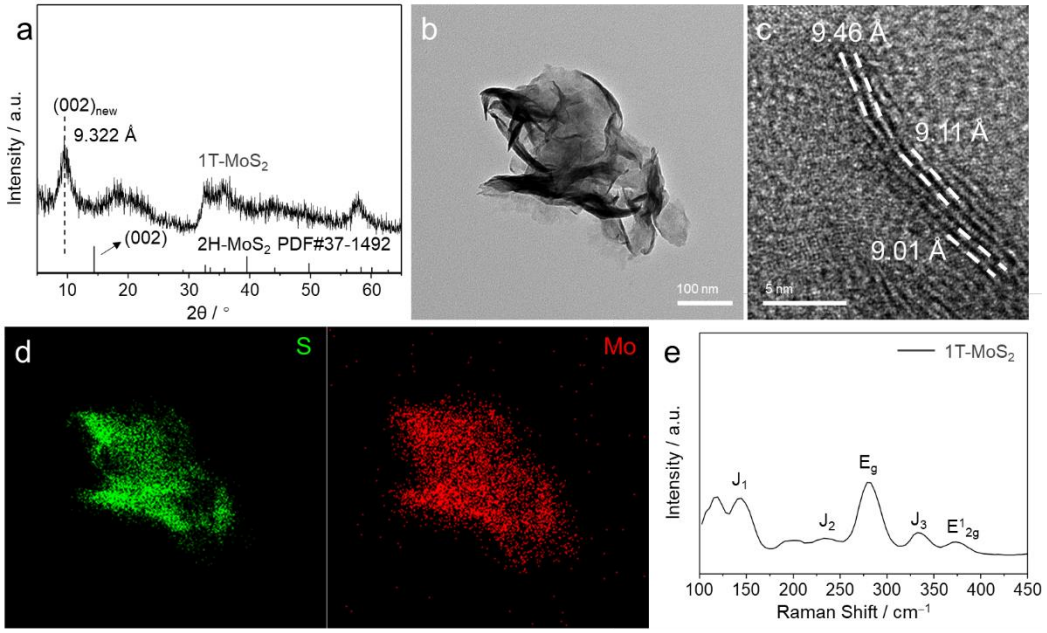


**Figure S2.** (**a**) XRD pattern, (**b**) TEM image, (**c**) HRTEM image, (**d**) EDS element mapping images of S, Mo, and (**e**) Raman spectra of 1T-$MoS_2$ nanosheets. Different with 2H phase (JCPDS card No. 37-1492), 002 peak of 1T phase shifted to a low angle of 9.48° (this is corresponding to an interlayer distance of 9.32 Å), and the second-order diffraction peak of 18.31° occurred simultaneously [1]. The d-spacing difference of 002 peak between the 2H and 1T phase is 3.17 Å, which is due to the intercalation of $NH_4^+$ between $MoS_2$ layers [2]. HRTEM shown the 1T-$MoS_2$ nanocrystals were composed of 3–6 layers, with the maximum interval of 9.46 Å, consistent with the XRD results. TEM mapping revealed the uniform distribution of Mo, S elements in the 1T-$MoS_2$ nanosheet. These results represent the successful synthesis of 1T-$MoS_2$.

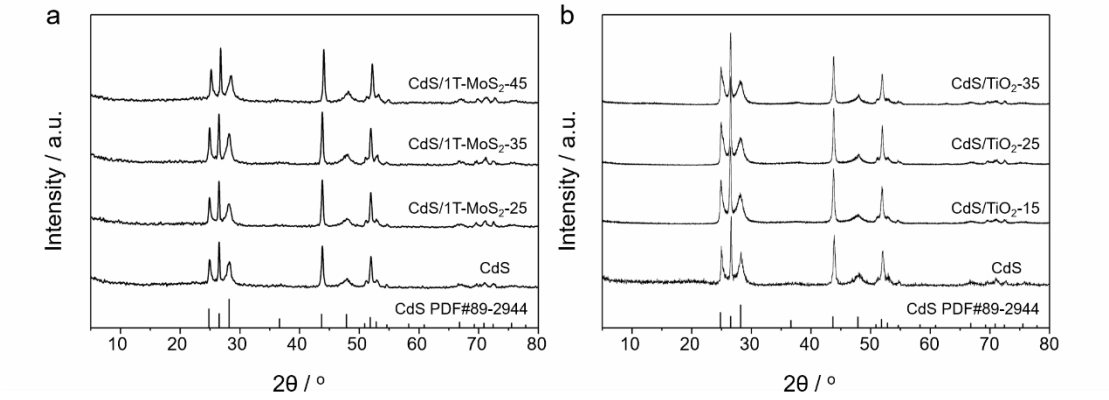


**Figure S3.** XRD patterns of binary heterojunctions CdS/1T-$MoS_2$ (**a**) and CdS/$TiO_2$ (**b**).

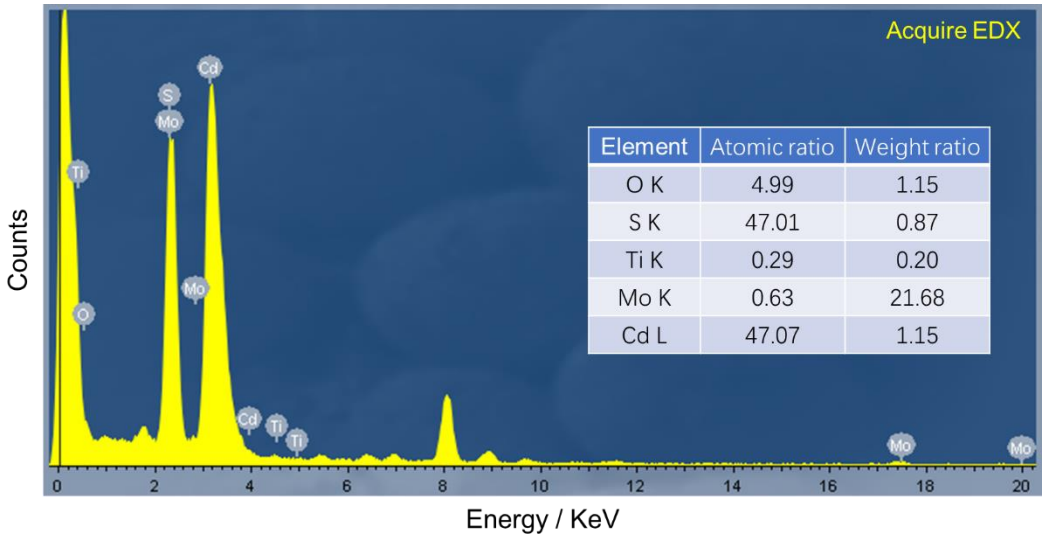


| Element | Atomic ratio | Weight ratio |
|---|---|---|
| O K | 4.99 | 1.15 |
| S K | 47.01 | 0.87 |
| Ti K | 0.29 | 0.20 |
| Mo K | 0.63 | 21.68 |
| Cd L | 47.07 | 1.15 |

**Figure S4.** EDS spectrum of CdS/1T-$MoS_2$/$TiO_2$-45-15 heterojunctions.

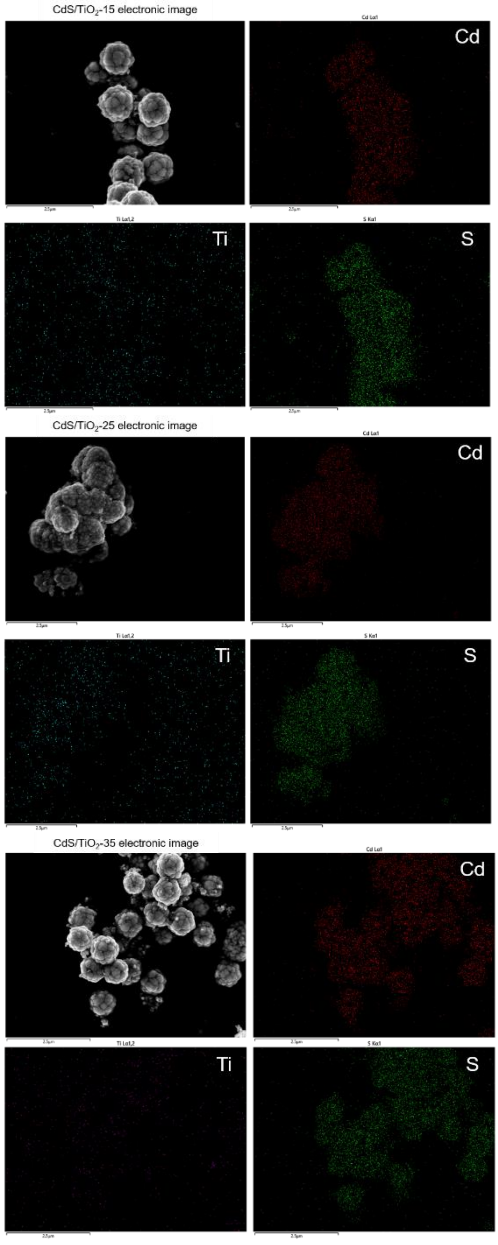

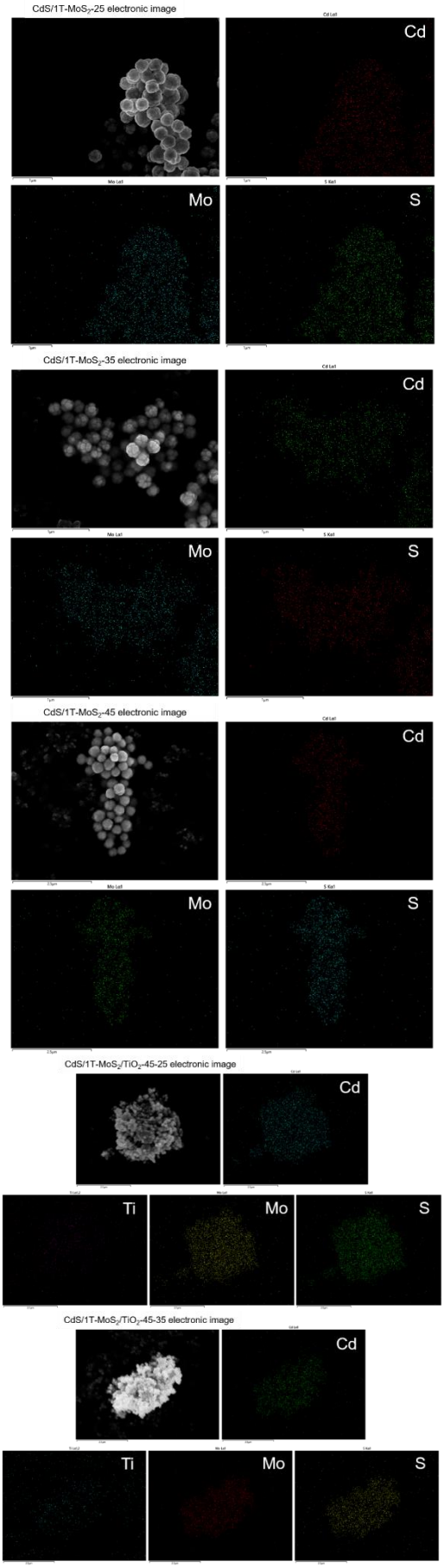
CdS/1T-MoS2-25 electronic image
Cd
Mo
S
CdS/1T-MoS2-35 electronic image
Cd
Mo
S
CdS/1T-MoS2-45 electronic image
Cd
Mo
S
CdS/1T-MoS2/TiO2-45-25 electronic image
Cd
Ti
Mo
S
CdS/1T-MoS2/TiO2-45-35 electronic image
Cd
Ti
Mo
S

**Figure S5.** SEM-EDS image of CdS/ $TiO_2$, CdS/1T-$MoS_2$ and CdS/1T-$MoS_2$/$TiO_2$. EDS element mapping shows the existence of Cd, S, Mo, Ti and their uniform distribution in the composites.

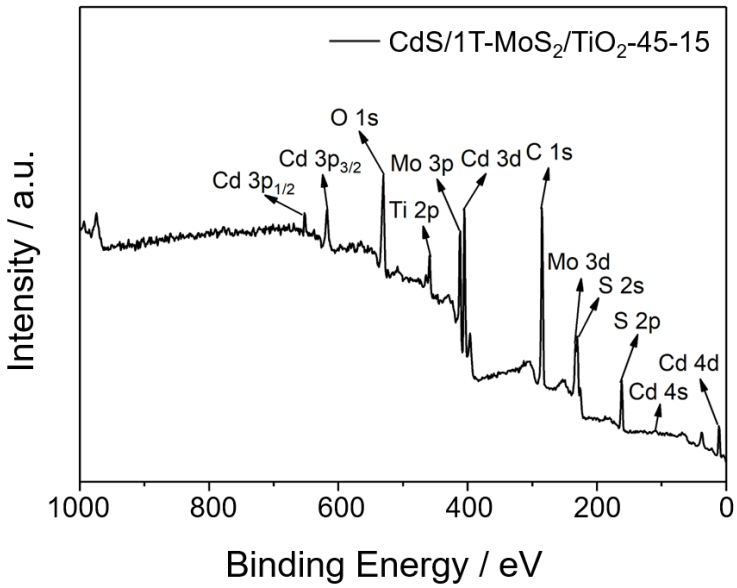


**Figure S6.** Full XPS spectrum of CdS/1T-$MoS_2$/$TiO_2$-45-15.

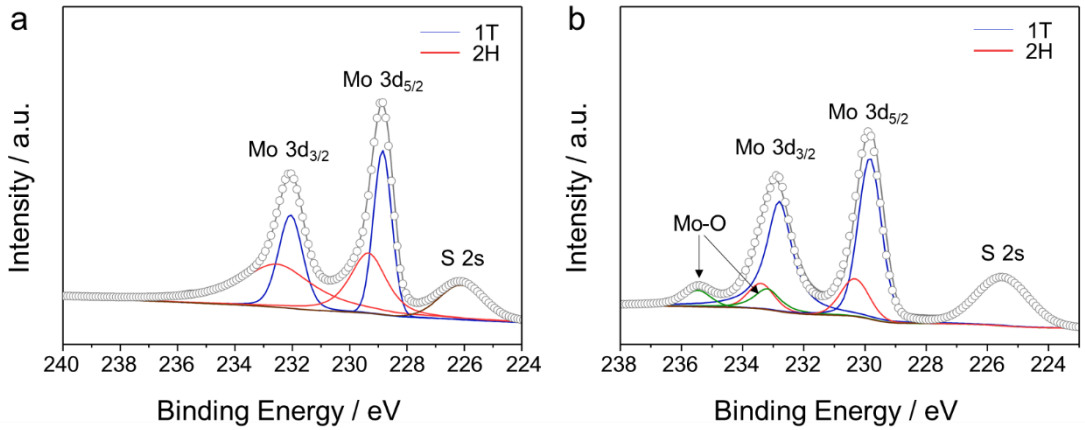


**Figure S7.** Deconvolutions of Mo 3d XPS analyses of 1T-$MoS_2$ (**a**) and CdS/1T-$MoS_2$/$TiO_2$-45-15 (**b**) samples.

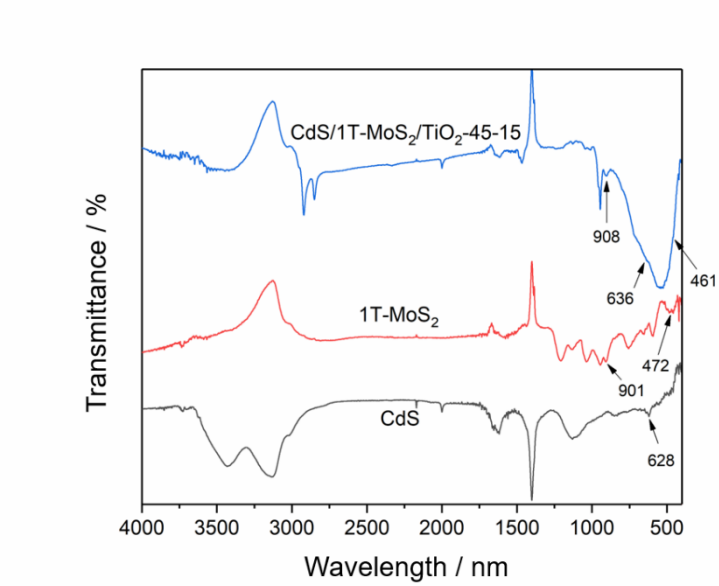


**Figure S8.** FTIR of pure CdS, 1T-$MoS_2$ and CdS/1T-$MoS_2$/$TiO_2$-45-15 nanocomposites. The IR characteristic peak of CdS at 628 $cm^{-1}$ is attributed to the stretching frequency of the Cd-S bond [3]. The peak around 472 $cm^{-1}$ was associated with Mo-S and the peaks at 901 $cm^{-1}$ were assigned to Mo-O vibrations of 1T-$MoS_2$ [4]. For CdS/1T-$MoS_2$/$TiO_2$-45-15, the corresponding Mo-S and Cd-S peaks were blue shifted. The characteristic peak at 461 $cm^{-1}$ is in accordance with the presence of Ti-O bond [5]. The Raman spectra (Figure 3a) also indicated that there are three the above-mentioned components in our composite.

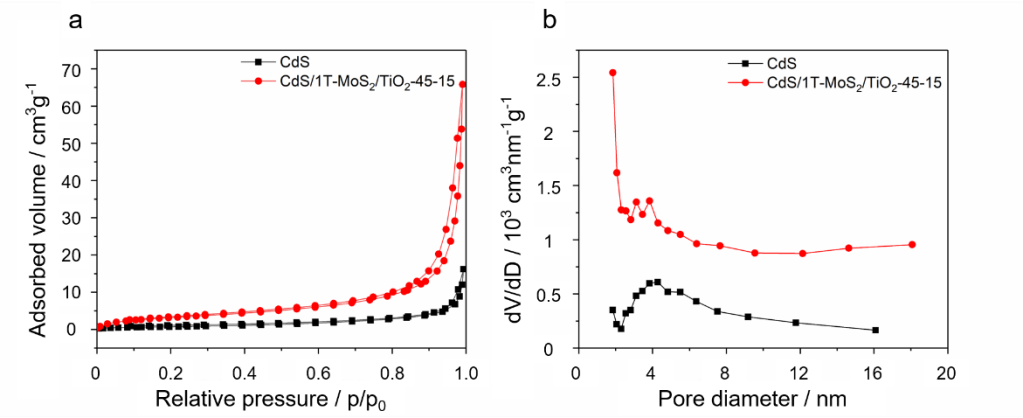


**Figure S9.** (**a**) Nitrogen sorption isotherms and (**b**) corresponding pore size distribution curves of CdS and CdS/1T-$MoS_2$/$TiO_2$-45-15. $N_2$ adsorption-desorption isotherms of CdS and CdS/1T-$MoS_2$/$TiO_2$ demonstrate a typical type-IV curve, indicating a mesoporous structure of the composite. Brunauer-Emmett-Teller surface area and pore size of CdS nanoparticles are calculated to be ≈2.85 $m^2$ $g^{-1}$ and 26.78 nm, respectively, which are smaller than that of CdS/1T-$MoS_2$/$TiO_2$ heterojunction (≈12.31 $m^2$ $g^{-1}$ and 31.43 nm, respectively), revealing the successful loading of 1T-$MoS_2$ and $TiO_2$ on the mesoporous CdS.

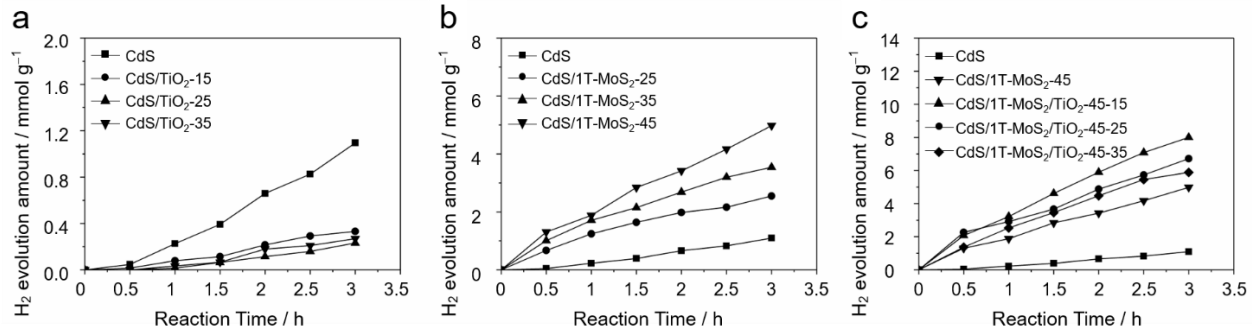

**Figure S10.** Total amount of photocatalytic hydrogen production in 3h of (**a**) CdS/$TiO_2$, (**b**) CdS/1T-$MoS_2$, and (**c**) CdS/1T-$MoS_2$/$TiO_2$.

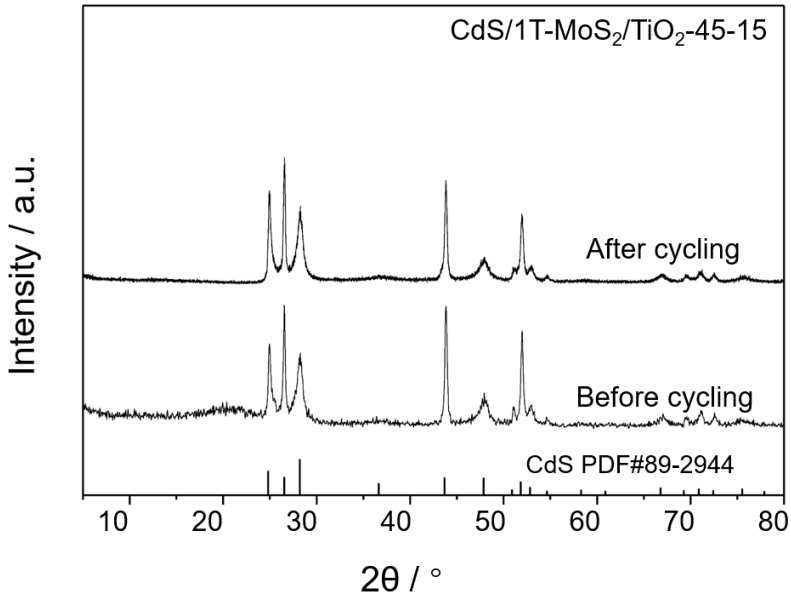


**Figure S11.** XRD pattern after hydrogen production cycle of CdS/1T-$MoS_2$/$TiO_2$-45-15.

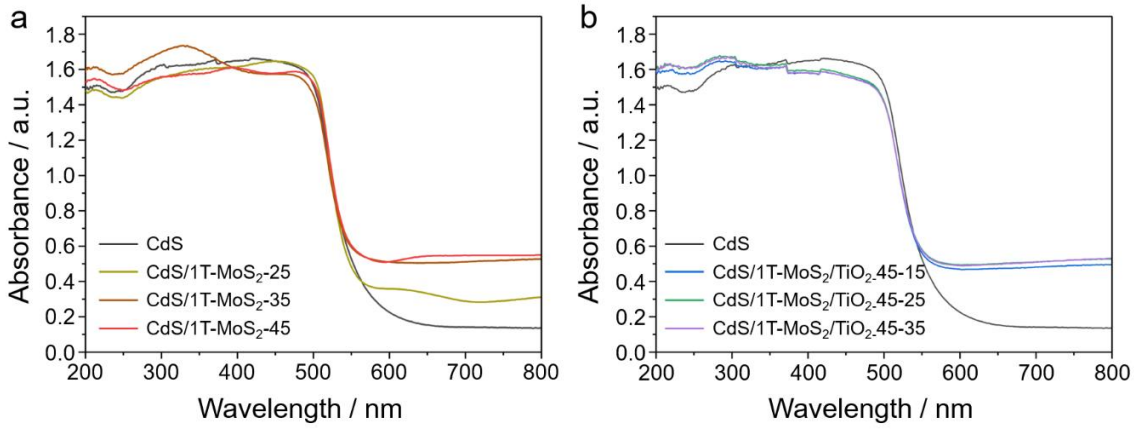


**Figure S12.** UV-vis diffuse reflectance spectra (DRS) of (**a**) binary CdS/1T-$MoS_2$ and (**b**) ternary CdS/1T-$MoS_2$/$TiO_2$.

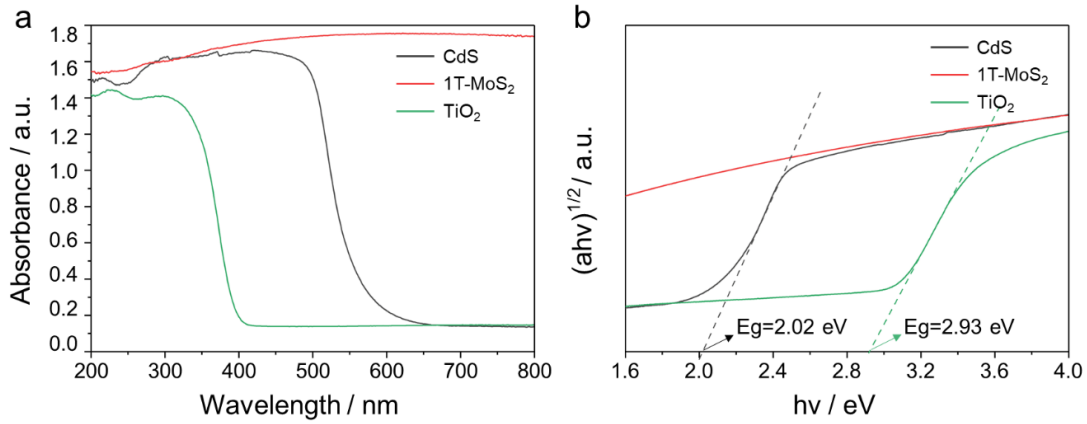


**Figure S13.** (**a**) UV-vis diffuse reflectance spectra (DRS) and (**b**) The plot of $(\alpha h\nu)^{1/2}$ vs photo energy ($h\nu$) of CdS, 1T-$MoS_2$ and $TiO_2$.

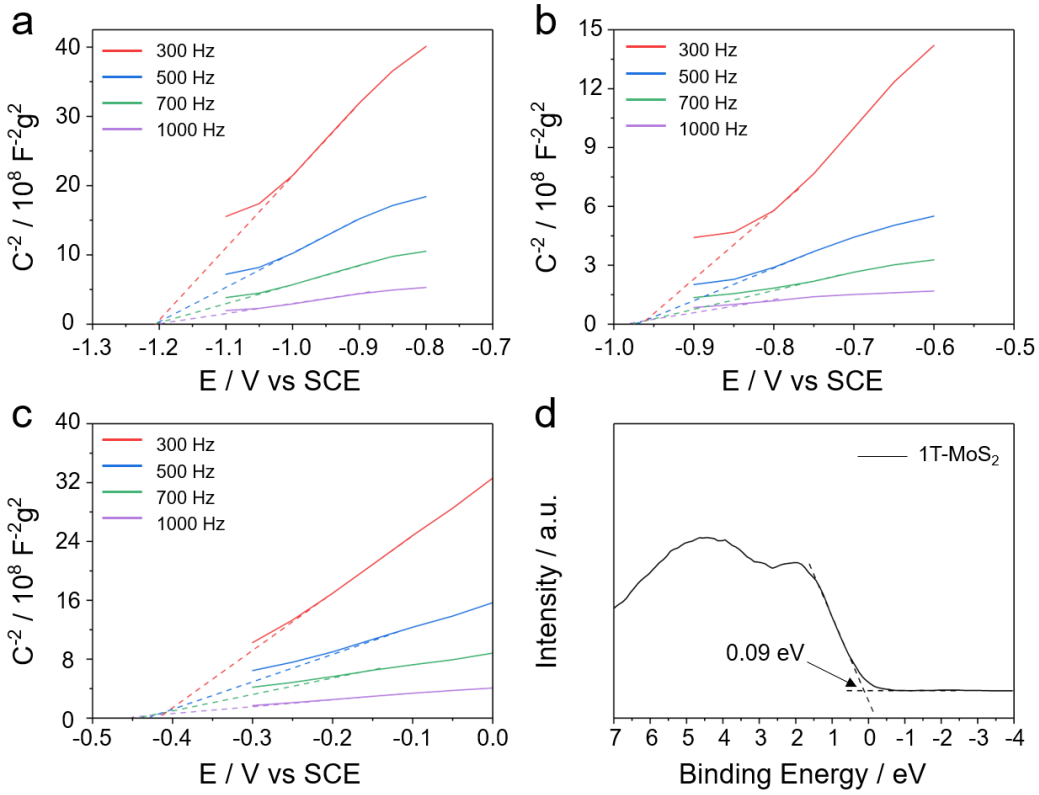


**Figure S14.** Mott-Schottky plots at different frequencies of (**a**) CdS, (**b**) $TiO_2$, and (**c**) 1T-$MoS_2$. (**d**) XPS-VB spectra of 1T-$MoS_2$.

## Reference

1. M.Wu.; J.Zhan.; K.Wu.; Z.Li.; L.Wang.; B.Geng.; L.Wang.; D.Pan.; *J. Mater. Chem. A* **2017**, *5* 14061–14069.
2. A.Anto.Jeffery.; C.Nethravathi.; M.Rajamathi.; *J. Phys. Chem. C* **2014**, *118*, 1386–1396.
3. L. Zhang.; X. Li.; Z. Mu.; J. Miao.; K. Wang.; R. Zhang.; S. Chen.; *RSC Advances* **2018**, *8*, 30747–30754.
4. J. Panda.; B. Tudu.; *AIP Conference Proceedings* **2018**, *1953*, 030127.
5. Mahalingam, T.; Selvakumar, C.; Ranjith Kumar, E.; Venkatachalam, T. *Physics Letters A* **2017**, *381*, 1815–1819.